Available online at www.sciencedirect.com
SCIENCE DIRECT®
PERGAMON
Automatica 39 (2003) 1583–1596
automatica
www.elsevier.com/locate/automatica

Nonlinear modelling and control of helicopters☆

J.C. Avila Vilchis[a], B. Brogliato[b,*], A. Dzul[c], R. Lozano[c]

[a] Universidad Autónoma del Estado de México, Facultad de Ingeniería 50130 Toluca, Mexico
[b] INRIA Rhône-Alpes ZIRST Montbonnot, 655 avenue de l'Europe 38334 Saint-Ismier, France
[c] Université de Technologie de Compiègne BP 20529, HEUDIASYC UMR CNRS 6599 60205, Compiègne cedex, France

Received 5 June 2001; received in revised form 12 February 2003; accepted 28 April 2003

Abstract

This paper presents the development of a nonlinear model and of a nonlinear control strategy for a VARIO scale model helicopter. Our global interest is a 7-DOF (degree-of-freedom) general model to be used for the autonomous forward-flight of helicopter drones. However, in this paper we focus on the particular case of a reduced-order model (3-DOF) representing the scale model helicopter mounted on an experimental platform. Both cases represent underactuated systems ($u \in \mathbb{R}^4$ for the 7-DOF model and $u \in \mathbb{R}^2$ for the 3-DOF model studied in this paper). The proposed nonlinear model possesses quite specific features which make its study an interesting challenge, even in the 3-DOF case. In particular aerodynamical forces result in input signals and matrices which significantly differ from what is usually considered in the literature on mechanical systems control. Numerical results and experiments on a scale model helicopter illustrate the theoretical developments, and robustness with respect to parameter uncertainties is studied.

Keywords: Nonlinear systems; Nonlinear control; Underactuated; Helicopter; Drone; Aerodynamics

1. Introduction

The interest for designing feedback controllers for various types of autonomous flying systems (so-called drones) has increased during the past decade due to important potential applications. Among these systems, helicopters constitute a very specific class due to their particular dynamical features (which make authors generally classify helicopters outside so-called VTOL aircrafts as in McCormick, 1995). The main difficulties (at a theoretical level) for designing stable feedback controllers for helicopters stem from their nonlinearities and couplings (for the solid mechanics part) and the fact that the inputs are not torques nor forces but displacements of some elements which enter the dynamics through aerodynamical forces/torques. This work is part of a project that concerns the modelling and control of a VARIO Benzin-Trainer scale model helicopter at the University of Technology of Compiègne, France (see photograph in Fig. 1). In this paper and in Avila-Vilchis (2001) the focus is on the derivation of a suitable model for control purpose, incorporating the main aerodynamical effects. Since it is not possible to provide all the detail of calculations that yield the form of the aerodynamical terms, in this paper we just indicate the general structure of the 3-DOF model. All calculations and hypotheses are described in detail in Avila-Vilchis (2001).

Helicopter vertical flight (take-off, climbing, hover, descent and landing) can be analyzed with the particular 3-DOF system obtained when the helicopter is mounted on an experimental platform. Although simplified, this 3-DOF Lagrangian model presents quite interesting control challenges due to nonlinearities, aerodynamical forces and underactuation. Though the mathematical model of this system is much simpler than that of the "free-flying" case, its dynamics will be shown to be non-trivial (nonlinear in the state, and underactuated). In Avila-Vilchis and Brogliato (2000) a specific nonlinear controller is proposed using the dissipativity properties of the model. Some other previous works have been developed for control problems in helicopters (Kaloust, Ham, & Qu, 1997; Kienitz, Wu, & Mansour, 1990; Koo, Hoffmann, Sinopoli, & Sastry,

☆ This paper was not presented at any IFAC meeting. This paper is recommended for publication in revised form by Associate Editor Henk Nijmeijer under the direction of Editor Hassan Khalil.

* Corresponding author.
E-mail addresses: jc_avila@uaemex.mx (J.C. Avila Vilchis), Bernard.Brogliato@inrialpes.fr (B. Brogliato), Alejandro.Dzul@hds.utc.fr (A. Dzul), Rogelio.Lozano@hds.utc.fr (R. Lozano).

0005-1098/03/$ - see front matter © 2003 Elsevier Ltd. All rights reserved.
doi:10.1016/S0005-1098(03)00168-7

Fig. 1. Vario Benzin-Trainer helicopter.

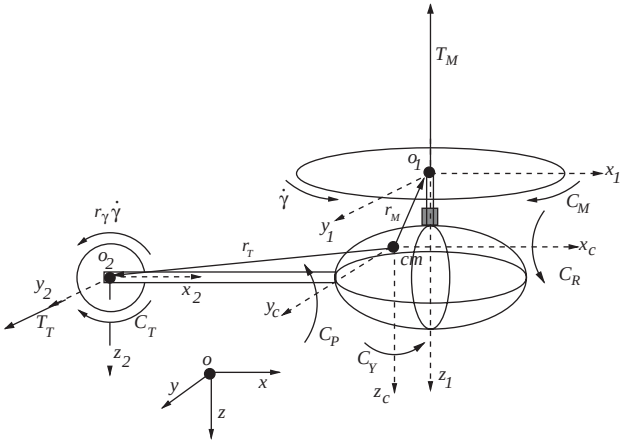

Fig. 2. Aerodynamical forces and torques.

1998; Koo & Sastry (1998); Mahony & Lozano, 1999; Mukherjee & Chen, 1993; Phillips, Karr, & Walker, 1996; Rozak & Ray, 1997; Shim, Koo, Hoffman, & Sastry, 1998; Sira-Ramírez, Zribi, & Ahmed, 1994). Contrary to most of the recent works in the field of nonlinear control of helicopters, we incorporate the main and tail rotors dynamics in the Lagrange equations. Moreover the control inputs are taken as the real helicopter inputs (the swashplate displacements of the main and tail rotors and the longitudinal and lateral cyclic pitch angles of the main rotor). This is shown to complicate significantly the way the input u appears in the Lagrange equations.

We present below a general panorama of the aerodynamic forces and torques acting on the helicopter. The helicopter center of mass (c.m.) in general is not located in a plane of symmetry. Some reference systems are then defined in Fig. 2 where the most important forces and torques acting on the helicopter are shown. T_M is the main rotor thrust, T_T is the tail rotor thrust, C_P is the pitching moment, C_R is the rolling moment, C_Y is the yaw moment, C_M is the main rotor drag torque, C_T is the tail rotor drag torque, [1] $\dot{\gamma}$ is the main rotor angular speed and r_γ is the gear ratio between the main and the tail rotors. In this paper we neglect the contributions of the horizontal and vertical stabilizers and the ground effects:

- The reference system (o,x,y,z) is an inertial one.
- The reference system (cm,x_c,y_c,z_c) is fixed at the center of mass of the helicopter and attached to its body.
- The reference system (o_1,x_1,y_1,z_1) is fixed and located at the center of the main rotor and attached to the helicopter body.
- The reference system (o_2,x_2,y_2,z_2) is fixed and located at the center of the tail rotor and attached to the helicopter body.

Due to the choice of the frames in Fig. 2, one has $\dot{\gamma} \leqslant 0$ for the VARIO helicopter. In this figure $r_M = [x_M \;\; y_M \;\; z_M]^T$ and $r_T = [x_T \;\; y_T \;\; z_T]^T$ represent the main and tail rotor center localization vectors with respect to the center of mass, respectively.

An experienced pilot can develop a relatively complicated take-off or free-flight (in 2D or 3D). However, helicopters often evolve in one of the three following flight modes. In each case the main rotor thrust orientation must allow one to compensate the pitch and roll torques that are produced on the helicopter by external perturbations. The tail rotor thrust magnitude variation will compensate the yaw torques of the same nature.

Hover: When the helicopter is climbing the pilot puts the helicopter on to fly at a certain height, normally OGE (out ground effect) where the thrust of the main rotor compensates the helicopter weight mg and the vertical drag force D_{vi} produced by the wake effect (the induced velocity acting on the fuselage). [2]

Vertical flight: This flight mode starts when the helicopter is at rest on the ground IGE (in ground effect). Then take-off is produced and the helicopter climbs. Vertical descent precedes landing. In the absence of perturbations the main rotor thrust is always vertical.

Forward flight: We consider that this flight mode will be OGE. The thrust of the main rotor has two component. The horizontal one or traction force ensures forward-flight and the vertical one keeps the helicopter at a constant height.

This paper is organized as follows. Section 2 is dedicated to the aerodynamical forces and torques acting on the helicopter and used in the 3-DOF Lagrangian model of the helicopter mounted on an experimental platform presented in Section 3. This model can be seen as made of two subsystems (translation and rotation). In Section 4 we present a linearizing control design for the reduced order model. Section 5 is devoted to simulation results and Section 6 for real time experiments of the helicopter-platform system. In Section 5 the robustness of the controller with respect to parametric uncertainties is studied. Finally we present

[1] All these quantities represent the magnitudes of the aerodynamic forces and torques.

[2] The wake effect is a very important one that is considered in the majority of aerodynamic analysis where for example the pitching-up transient phenomenon produced by the induced velocity has been studied (see Tchen-Fo, Allain, & Desopper, 2000 for example).

some conclusions in Section 7. We provide a glossary of aerodynamical terms in Appendix A.

2. Aerodynamical forces

Algebraic expressions of the aerodynamical forces and torques are used to deduce the generalized external forces acting on the helicopter. In this section a brief presentation of the forces and torques computing is provided with the interest to show what the nature of these forces and torques is. The blade element method (Prouty, 1995; Stepniewsky, 1984) is used. See Appendix A for the explanation of the used terms.

For a blade differential element the incremental lift force ΔL is

$$\Delta L = P_{\mathrm{d}} c_{\mathrm{l}} c \Delta r_e = \frac{\rho}{2} V_{\mathrm{T}}^2 a \alpha c \Delta r_e \tag{1}$$

where P_{d} is the dynamical pressure, c_{l} is the lift coefficient, ρ is the air density, V_{T} is the signed value of the tangent velocity to the blade element chord, a is the slope of the lift curve, c is the chord of the blade, α is the angle of attack of the blade element and Δr_e is the incremental radial distance (see Fig. 3).

The following assumptions are taken into account in this development:

- Twist, attack, slide and flapping angles, flight velocity and the control inputs are independent of γ and of r_e (see Eq. (4) and Figs. 3 and 4).
- $\sin(\beta) \approx \beta$ where β is the flapping angle.
- $\imath_e = \arctan(V_{\mathrm{P}}/V_{\mathrm{T}}) \approx V_{\mathrm{P}}/V_{\mathrm{T}}$ where $\imath_e$ is the incidence angle (see Fig. 5).

The total thrust is equal to the number of blades (p) times the average lift per blade:

$$\begin{aligned} T_{\mathrm{M}} &= \frac{p}{2\pi} \int_0^{2\pi} \int_0^{R_{\mathrm{M}}} \frac{\Delta L}{\Delta r_e} \, \mathrm{d}r_e \, \mathrm{d}\gamma \\ &= \frac{\rho p a c}{4\pi} \int_0^{2\pi} \int_0^{R_{\mathrm{M}}} V_{\mathrm{T}}^2 \alpha \, \mathrm{d}r_e \, \mathrm{d}\gamma, \end{aligned} \tag{2}$$

where R_{M} is the radius of the main rotor. The angle of attack α is given by Eq. (3) (Prouty, 1995), where φ is the pitch angle defined in (4) and V_{P} is the velocity signed value that represents the perpendicular velocity to the blade quarter-chord line and lies in a plane that contains the rotor shaft (see Fig. 4).

$$\alpha = \varphi + \arctan\left(\frac{V_{\mathrm{P}}}{V_{\mathrm{T}}}\right), \tag{3}$$

$$\varphi(r_e, \gamma, u) = \varphi_0 + \frac{r_e}{R_{\mathrm{M}}} \varphi_1 - u_4 \cos(\gamma) - u_3 \sin(\gamma). \tag{4}$$

In (4) φ_0 is the average pitch at the center of rotation, φ_1 is the blade linear twist angle and inputs u_4 and u_3 are the lateral and longitudinal cyclic pitch angles of the main rotor, respectively.

We can now write:

$$T_{\mathrm{M}} = \frac{\rho p a c}{4\pi} \int_0^{2\pi} \int_0^{R_{\mathrm{M}}} [V_{\mathrm{T}}^2 \varphi + V_{\mathrm{T}} V_{\mathrm{P}}] \, \mathrm{d}r_e \, \mathrm{d}\gamma. \tag{5}$$

In the (o_1, x_1, y_1, z_1) reference system (see Fig. 2) the thrust vector is given by Eq. (6).

$$\vec{T}_{\mathrm{M}} = \begin{bmatrix} T_{\mathrm{M}} \sin(u_3) \cos(u_4) \\ T_{\mathrm{M}} \cos(u_3) \sin(u_4) \\ T_{\mathrm{M}} \cos(u_3) \cos(u_4) \end{bmatrix} \tag{6}$$

with T_{M} given in (5). For the 3-DOF model $u_3 = u_4 = 0$ so $\vec{T}_{\mathrm{M}} = [0\,0\,T_{\mathrm{M}}]^{\mathrm{T}}$. For the blade element drag torque we consider Eq. (7) and Fig. 5.

$$\Delta C_{\mathrm{M}} = (\Delta D \cos(\imath_e) + \Delta L \sin(\imath_e)) r_e, \tag{7}$$

where $\Delta D \cos(\imath_e)$ is the profile incremental drag force, $\Delta L \sin(\imath_e)$ is the induced incremental drag force due to the tilt of the lift vector (helicopters fly the nose down). Since $\imath_e \ll 1$ the influence of $\Delta D \sin(\imath_e)$ in T_{M} has been neglected in (5).

Taking into account Eq. (3), the number of blades, the blade element conditions and the total contribution in one revolution we can write:

$$C_{\mathrm{M}} = \frac{\rho p a c}{4\pi} \int_0^{2\pi} \int_0^{R_{\mathrm{M}}} \left[\frac{c_{\mathrm{d}}}{a} V_{\mathrm{T}}^2 + V_{\mathrm{P}}^2 + V_{\mathrm{T}} V_{\mathrm{P}} \varphi\right] r_e \, \mathrm{d}r_e \, \mathrm{d}\gamma, \tag{8}$$

where c_{d} is the drag coefficient. In a similar way we can write expressions for the thrust and drag torque of the tail rotor (Eqs. (9) and (10)) where t and T stand for tail rotor. Horizontal forces or simply H-forces are not taken into account in this modelling task. H-forces are the drag forces produced by the wind over the main and tail rotors when the helicopter is in forward flight mode:

$$T_{\mathrm{T}} = \frac{\rho p_{\mathrm{t}} a c_{\mathrm{t}}}{4\pi} \int_0^{2\pi} \int_0^{R_{\mathrm{t}}} [V_{\mathrm{T}}^2 \varphi + V_{\mathrm{T}} V_{\mathrm{P}}]_{\mathrm{t}} \, \mathrm{d}r_e \, \mathrm{d}(r_\gamma \gamma), \tag{9}$$

$$C_{\mathrm{T}} = \frac{\rho p_{\mathrm{t}} c_{\mathrm{t}} a}{4\pi} \int_0^{2\pi} \int_0^{R_{\mathrm{T}}} \left[\frac{c_{\mathrm{dt}}}{a} + \alpha \frac{V_{\mathrm{P}}}{V_{\mathrm{T}}}\right]_{\mathrm{t}} V_{\mathrm{T}}^2 r_e \, \mathrm{d}r_e \, \mathrm{d}(r_\gamma \gamma). \tag{10}$$

For the computing of aerodynamic forces and torques only the inplane velocity V_{T} that is perpendicular to the blade attack side and the V_{P} velocity are taken into account (Prouty, 1995; Stepniewsky, 1984). For the main rotor we have:

$$V_{\mathrm{T}} = V \cos(\alpha_s) \sin(\gamma - \delta) + \dot{\gamma} r_e. \tag{11}$$

The velocity V_{P} is formed by several terms:

$$\begin{aligned} V_{\mathrm{P}} = v_{\mathrm{local}} &- V \sin(\alpha_s) - r_e \dot{\beta} \\ &+ V \cos(\alpha_s) \cos(\delta) \sin(\beta) \cos(\gamma) \end{aligned} \tag{12}$$

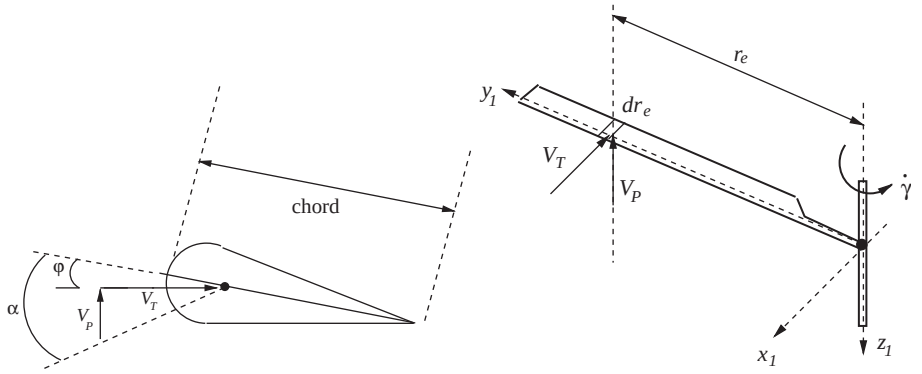

Fig. 3. Tangential and perpendicular velocities.

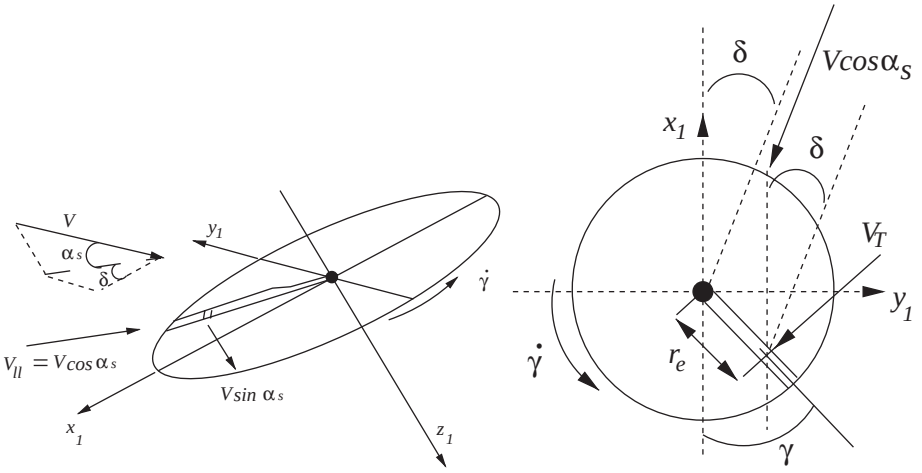

Fig. 4. Main rotor inplane velocity.

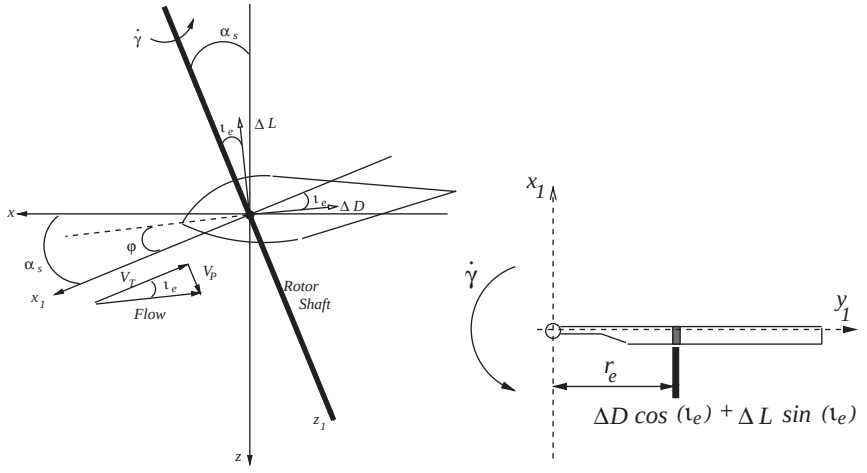

Fig. 5. Drag torque of the main rotor.

where v_{local} is the local induced velocity,[3] $V\sin(\alpha_s)$ is the perpendicular component of the flight velocity, $r_e\dot{\beta}$ is the contribution of the vertical flapping motion and $V\cos(\alpha_s)\cos(\delta)\sin(\beta)\cos(\gamma)$ is the effect of the flight velocity component on the rotation plane of the main rotor (acting on the wing upper surface when $\gamma = 0$ and on the wing bottom surface when $\gamma = -\pi$).

When $\delta = 0$ and α_s is small the general expressions obtained in Avila-Vilchis (2001) for aerodynamic forces and torques become those proposed by Prouty (1995) in the forward flight case. Moreover, when $V = 0$ these expressions reduce to those of the hover mode.

3. The 3-DOF model

We consider Fig. 6 where the VARIO helicopter mounted on an experimental platform is represented. It is important to say that in this particular case the helicopter is in an OGE[4] condition. The effects of the compressed air in take-off and landing are then neglected.

In Fig. 6 the counterbalance weight compensates the weight of the vertical column of the platform. The xyz reference system is an inertial one and the $x_c y_c z_c$ reference system is a body fixed frame. The model is obtained by a Lagrangian formulation. The kinetic energy T is formed by four quantities: T_{t}, T_{rF}, T_{rM} and T_{rT} corresponding to the translational kinetic energy and the rotational kinetic energy of the fuselage, of the main and of the tail rotors, respectively. The potential energy is formed by the gravitational potential energy U_{g} and by the elastic potential energy U_{b} associated with vertical flapping. In the particular case that we present here $U_{\text{b}} = ka_0^2$ where k is the stiffness of the main rotor blades and a_0 is the coning angle (see Fig. 7). The model has the form:

$$M(q)\ddot{q} + C(q,\dot{q})\dot{q} + G(q) = Q(u), \tag{13}$$

where $M(q) \in \mathbb{R}^{3\times 3}$ is the inertia matrix, $C(q,\dot{q}) \in \mathbb{R}^{3\times 3}$ is the Coriolis matrix, $G(q) \in \mathbb{R}^3$ is the vector of conservative forces, $Q(u) = [f_z \;\; \tau_z \;\; \tau_\gamma]^{\text{T}}$ is the vector of generalized forces, $q = [z \;\; \phi \;\; \gamma]^{\text{T}}$ is the vector of generalized coordinates and $u = [h_{\text{M}} \;\; h_{\text{T}}]^{\text{T}}$ is the vector of control inputs. Here f_z, τ_z and τ_γ are the vertical force, the yaw torque and the main rotor torque, respectively. The height $z < 0$ upwards, ϕ is the yaw angle and γ is the main rotor azimuth angle. The Lagrange development for this 3-DOF model defining the structure of $M(q)$, $C(q,\dot{q})$ and $G(q)$ can be found in Avila-Vilchis, Brogliato, and Lozano (2000).

[3] Expressions to calculate the induced velocity in hover, in vertical and in forward flight can be found in Prouty (1995). In Avila-Vilchis (2001) one more general expression to calculate the induced velocity for a more general 3D flight mode is provided.

[4] The platform height is greater than the main rotor diameter so we consider that the helicopter is OGE (Out Ground Effect).

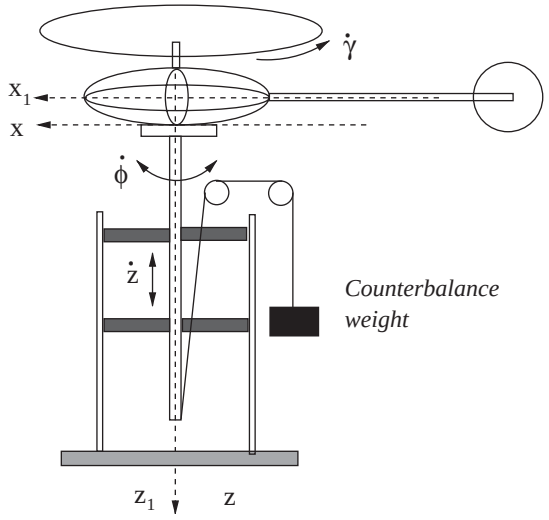

Fig. 6. Helicopter-platform.

The Lagrangian L is given by

$$L = \tfrac{1}{2}m\dot{z}^2 + \tfrac{1}{2}I_{zz\text{F}}\dot{\phi}^2 + \tfrac{1}{2}I_{zz\text{M}}(\dot{\phi}+\dot{\gamma})^2 + \tfrac{1}{2}I_{zz\text{T}}\dot{\phi}^2 + \tfrac{1}{2}I_{yy\text{T}}\dot{\gamma}^2 r_\gamma^2 + mgz - ka_0^2 \tag{14}$$

and we have:

$$M(q) = \begin{bmatrix} c_0 & 0 & 0 \\ 0 & c_1 + c_2\cos^2(c_3\gamma) & c_4 \\ 0 & c_4 & c_5 \end{bmatrix},$$

$$C(q,\dot{q}) = \begin{bmatrix} 0 & 0 & 0 \\ 0 & c_6\sin(2c_3\gamma)\dot{\gamma} & c_6\sin(2c_3\gamma)\dot{\phi} \\ 0 & -c_6\sin(2c_3\gamma)\dot{\phi} & 0 \end{bmatrix},$$

$$G(q) = \begin{bmatrix} c_7 \\ 0 \\ 0 \end{bmatrix}. \tag{15}$$

The c_i's $i = 0,\ldots,7$ are the physical constants given in Table 1. The swashplate displacements of the main (h_{M}) and tail (h_{T}) rotors are proportional to their respective collective pitch angle φ_0 (see Eq. (16) and Fig. 7):

$$[\varphi_0]_k = \arctan\left(\frac{u_j}{bl_i}\right) \approx \frac{u_j}{bl_i}, \tag{16}$$

where if $j = 1$ then $i = m$ and $k = M$, if $j = 2$ then $i = t$ and $k = T$. Here M and m stand for main-rotor and T and t for tail-rotor. The lever arm bl_i is shown in Fig. 7.

The components of the vector Q take the particular form (17) (Avila-Vilchis, 2001): $f_z = T_{\text{M}} + D_{\text{vi}}$, $\tau_z = T_{\text{T}}x_{\text{T}}$ and $\tau_\gamma = C_{\text{M}} + C_{\text{mot}}$. Here C_{mot} is the engine torque that we assume proportional to the first control input ($C_{\text{mot}} = K_{\text{mot}}u_1$). The

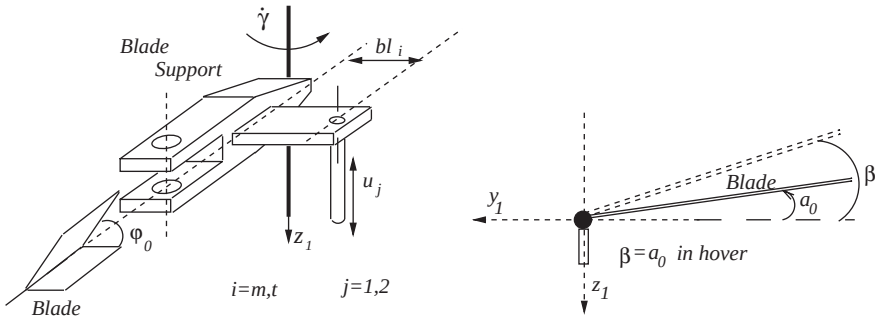

Fig. 7. bl_i for $i = m, t$ and the coning angle.

Table 1
3-DOF model parameters

c_i	Numerical value	c_i	Numerical value
c_0	7.5 kg	c_8	3.411 kg
c_1	0.4305 kg m^2	c_9	0.6004 kg m/s
c_2	3×10^{-4} kg m^2	c_{10}	3.679 N
c_3	−4.143	c_{11}	−0.1525 kg m
c_4	0.108 kg m^2	c_{12}	12.01 kg m/s
c_5	0.4993 kg m^2	c_{13}	1×10^5 N
c_6	-6.214×10^{-4} kg m^2	c_{14}	1.206×10^{-4} kg m^2
c_7	−73.58 N	c_{15}	2.642 N

generalized forces vector is given by

$$Q(u) = \begin{bmatrix} c_8\dot{\gamma}^2 u_1 + c_9\dot{\gamma} + c_{10} \\ c_{11}\dot{\gamma}^2 u_2 \\ (c_{12}\dot{\gamma} + c_{13})u_1 + c_{14}\dot{\gamma}^2 + c_{15} \end{bmatrix}. \tag{17}$$

For the 3-DOF model ($\delta = \alpha_s = 0$, $V = \dot{z}$) and with the assumption that the helicopter evolves at low rates of vertical velocity so that the vertical flight induced velocity (v_v) and the hover induced velocity (v_h) are approximately equal, the algebraic values of the main and tail rotor thrust and of the main rotor drag torque take the forms

$$T_M(\dot{\gamma}, u_1) = c_8\dot{\gamma}^2 u_1 + c_9\dot{\gamma}, \tag{18}$$

$$T_T(\dot{\gamma}, u_2) = c_{11}\dot{\gamma}^2 u_2, \tag{19}$$

$$C_M(\dot{\gamma}, u_1) = c_{12}\dot{\gamma}u_1 + c_{14}\dot{\gamma}^2 + c_{15}. \tag{20}$$

Modelling the generalized forces vector as $Q(u) = A(\dot{q})u + B(\dot{q})$ and from (17) we can write:

$$A(\dot{q}) = \begin{bmatrix} c_8\dot{\gamma}^2 & 0 \\ 0 & c_{11}\dot{\gamma}^2 \\ c_{12}\dot{\gamma} + c_{13} & 0 \end{bmatrix}, \tag{21}$$

$$B(\dot{q}) = \begin{bmatrix} c_9\dot{\gamma} + c_{10} \\ 0 \\ c_{14}\dot{\gamma}^2 + c_{15} \end{bmatrix}.$$

The c_i's $i = 8, \ldots, 15$ are the aerodynamical constants given in Table 1. The values and definitions of all the helicopter parameters can be consulted in Avila-Vilchis (2001).

Remark 1. The motor dynamics is slower than that of the main rotor. However, in scale model helicopters there is a coupling between the motor power and the main rotor blade collective pitch angle by the u_1 input as a consequence of handling conditions. The fact that in some real helicopters the motor power is associated with an independent third input (the throttle lever) would represent for the helicopter-platform model a completely actuated system.

Remark 2. The main rotor thrust T_M or $\dot{\gamma}$ are not used as inputs in (17) because $\ddot{\gamma}$ is very small due to the motor capabilities. Given that $\dot{u_1}$ and $\dot{u_2}$ can be larger than $\ddot{\gamma}$, u_1 and u_2 are preferred as inputs.

Remark 3. The dynamics in (13) (17) differs in several aspects from the canonical form for underactuated systems studied in Reyhanoglu, Van der Schaft, McClamroch, and Kolmanovsky (1999). In particular the form of the matrix multiplying the input is not the same. As a consequence the results on stabilization to an equilibrium point $(q^e, 0)$ that can be found in Reyhanoglu et al. (1999) (Proposition 1) do not apply for (13) (17), since for an helicopter it is highly desirable to keep $|\ddot{\gamma}| \gg 1$ and even to obtain $\dot{\gamma} \approx$ constant during the flight.

4. Control design

In the following we assume that initially $|\ddot{\gamma}(0)| \geqslant \delta > 0$ and $z(0) < 0$. The operation is split into two main phases:

Phase 1 (*Start up and take-off*): In this phase we assume that the main rotor is rotating ($\dot{\gamma} \neq 0$). The feedback control has to guarantee asymptotic stability of the tracking errors $\tilde{z} = z - z_d(t)$, $\dot{\tilde{z}} = \dot{z} - \dot{z_d}(t)$, $\tilde{\phi} = \phi - \phi_d(t)$ and $\dot{\tilde{\phi}} = \dot{\phi} - \dot{\phi_d}(t)$ when the helicopter is at rest on the ground. Moreover the controller has to assure that the helicopter takes-off.

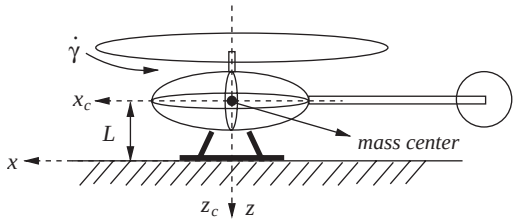

Fig. 8. Mass center localization.

Phase 2 (*Vertical flight*): When the helicopter takes-off ($z < L - \varepsilon$ for some $\varepsilon > 0$. See Fig. 8), the controller guarantees the asymptotic tracking of the preceding errors while $\dot{\gamma}$ converges to a constant value and remains bounded away from 0.

The robustness properties with respect to uncertainties on the parameters a (the slope of the lift curve), c_d (the drag coefficient) and K_{mot} (the motor gain) will be numerically studied by computing the quadratic criterion

$$J = \int_0^{t_f} [|\tilde{z}|^2 + |\dot{\tilde{z}}|^2 + |\tilde{\phi}|^2 + |\dot{\tilde{\phi}}|^2 + u^T u]\,dt \tag{22}$$

In this criterion t_f is the final time of simulation. In J in (22) $\tilde{\gamma}$ and $\dot{\tilde{\gamma}}$ are not included since even when the main rotor is turning, we do not require any tracking property in this variables.

From (13), taking into account (17) and (15) and since the ground constraint is a unilateral constraint $z - L \leqslant 0$ the helicopter dynamical model can be written as:

$$\ddot{q} = M^{-1}(q)(-C(q,\dot{q})\dot{q} - G(q) + Q(u) - \nabla g\lambda),$$
$$z - L \leqslant 0, \quad \lambda \geqslant 0, \quad \lambda(z - L) = 0, \tag{23}$$

where $\nabla g = (\partial[z-L]/\partial q) = [1\ \ 0\ \ 0]^T$ and $\lambda \geqslant 0$ is a Lagrange multiplier. Assuming respectively, that $z - L = 0$ and $z - L = \dot{z} = 0$ in strictly positive time intervals, from (23) we get:

$$\ddot{q} = M^{-1}(q)(-C(q,\dot{q})\dot{q} - G(q) + Q(u) - \nabla g\lambda),$$
$$\ddot{z} \leqslant 0, \quad \lambda \geqslant 0, \quad \lambda\ddot{z} = 0. \tag{24}$$

In an explicit way we have for $\ddot{q}$ in (24):

$$\ddot{z} = \frac{1}{c_0}[c_8\dot{\gamma}^2 u_1 + c_9\dot{\gamma} + c_{10} - c_7 - \lambda],$$

$$\ddot{\phi} = \frac{1}{D(\gamma)}[c_5(c_{11}\dot{\gamma}^2 u_2 - 2c_6\sin(2c_3\gamma)\dot{\gamma}\dot{\phi}) - c_4((c_{12}\dot{\gamma} + c_{13})u_1 + c_6\sin(2c_3\gamma)\dot{\phi}^2 + c_{14}\dot{\gamma}^2 + c_{15})], \tag{25}$$

$$\ddot{\gamma} = \frac{1}{D(\gamma)}[-c_4(c_{11}\dot{\gamma}^2 u_2 - 2c_6\sin(2c_3\gamma)\dot{\gamma}\dot{\phi}) + (c_1 + c_2\cos^2(c_3\gamma))((c_{12}\dot{\gamma} + c_{13})u_1 + c_6\sin(2c_3\gamma)\dot{\phi}^2 + c_{14}\dot{\gamma}^2 + c_{15})],$$

where $D(\gamma) = c_1c_5 - c_4^2 + c_2c_5\cos^2(c_3\gamma)$. If in the first equation of (25) $\ddot{z} = 0$ ($\lambda > 0$ $z - L = 0$ $z_0 = L$), then:

$$\lambda = c_8\dot{\gamma}^2 u_1 + c_9\dot{\gamma} + c_{10} - c_7 \tag{26}$$

and if $\ddot{z} < 0$ ($\lambda = 0$ $z - L < 0$), then:

$$\ddot{z} = \frac{1}{c_0}[c_8\dot{\gamma}^2 u_1 + c_9\dot{\gamma} + c_{10} - c_7]. \tag{27}$$

Conditions $\ddot{z} = 0$ and $\ddot{z} < 0$ represent the constrained and free-flight modes of the system, respectively. While $\lambda > 0$ the helicopter is at rest on the ground. Take-off is possible only when $\lambda = 0$.

We propose to use the control:

$$u_1 = \frac{1}{c_8\dot{\gamma}^2}[c_7 - c_{10} - c_9\dot{\gamma} + c_0(\ddot{z}_d - \lambda_1\dot{\tilde{z}} - \lambda_2\tilde{z})],$$

$$u_2 = \frac{1}{c_5c_{11}\dot{\gamma}^2}[D(\gamma)(\ddot{\phi}_d - \lambda_3\dot{\tilde{\phi}} - \lambda_4\tilde{\phi}) + 2c_5c_6\sin(2c_3\gamma)\dot{\gamma}\dot{\phi} + c_4((c_{12}\dot{\gamma} + c_{13})u_1 + c_6\sin(2c_3\gamma)\dot{\phi}^2 + c_{14}\dot{\gamma}^2 + c_{15})]. \tag{28}$$

Hence the closed-loop system becomes (see Eq. (25)):

$$0 = \ddot{\tilde{z}} + \lambda_1\dot{\tilde{z}} + \lambda_2\tilde{z},$$
$$0 = \ddot{\tilde{\phi}} + \lambda_3\dot{\tilde{\phi}} + \lambda_4\tilde{\phi}, \tag{29}$$

$$\ddot{\gamma} = \frac{1}{D(\gamma)}[-c_4(c_{11}\dot{\gamma}^2 u_2 - 2c_6\sin(2c_3\gamma)\dot{\gamma}\dot{\phi}) + (c_1 + c_2\cos^2(c_3\gamma))((c_{12}\dot{\gamma} + c_{13})u_1 + c_6\sin(2c_3\gamma)\dot{\phi}^2 + c_{14}\dot{\gamma}^2 + c_{15})],$$

where the $(\gamma, \dot{\gamma})$-dynamics represents the zero-dynamics of (25) with inputs u_1, u_2 and output $(z,\ \phi)$. Using Eqs. (28) in the last equation of (29) we have after simplifications:

$$\ddot{\gamma} = a_1\sin(2c_3\gamma)\dot{\phi}^2 + a_2\dot{\gamma}^2 + \frac{a_3}{\dot{\gamma}} + \frac{a_4}{\dot{\gamma}^2} + \left(\frac{a_5}{\dot{\gamma}} + \frac{a_6}{\dot{\gamma}^2}\right)\ddot{z}_d + a_7\ddot{\phi}_d + a_8, \tag{30}$$

where $a_1 = c_6/c_5$, $a_2 = c_{14}/c_5$, $a_3 = ((c_7 - c_{10})c_{12} - c_9c_{13})/c_5c_8$, $a_4 = (c_7 - c_{10})c_{13}/c_5c_8$, $a_5 = c_0c_{12}/c_5c_8$, $a_6 = c_0c_{13}/c_5c_8$, $a_7 = -c_4/c_5$ and $a_8 = (c_8c_{15} - c_9c_{12})/c_5c_8$. If the desired trajectories and initial data are chosen in such a way that terms including $\dot{\phi}^2$, $\ddot{z}_d$ and $\ddot{\phi}_d$ can be neglected we have the following simplified time-invariant equation:

$$\ddot{\gamma} = a_2\dot{\gamma}^2 + \frac{a_3}{\dot{\gamma}} + \frac{a_4}{\dot{\gamma}^2} + a_8. \tag{31}$$

Analyzing the values of angular velocity from which the angular acceleration is zero in (31) we can write:

$$a_2\dot{\gamma}^4 + a_8\dot{\gamma}^2 + a_3\dot{\gamma} + a_4 = 0, \tag{32}$$

where $a_2 = 2.415 \times 10^{-4}$, $a_8 = 1.057$, $a_3 = -35797.919$ and $a_4 = -4536341.8$ (see Table 1 for parametric constant

values). The solutions of (32) are $\dot{\gamma}^* = 563.68, -219.53 \pm 468.2i$ and -124.62 rad/s. Only the last of these values $\dot{\gamma}^* = -124.62$ rad/s has a physical meaning for the system (see Fig. 2 for the rotation sense of the main rotor).

The $\dot{\gamma}$-dynamics (31), linearized around the equilibrium point of interest $\dot{\gamma}^* = -124.62$, has a real eigenvalue equal to -2.44. As a consequence, all trajectories starting sufficiently near $\dot{\gamma}^*$ converge to the latter (see Khalil, 1996).

It then follows that the zero-dynamics in (29) has a stable behavior. Simulation results of (29) (see Section 5) show that $\dot{\gamma}$ remains bounded away from zero during the flight. For the chosen trajectories and gains $\dot{\gamma}$ converges rapidly to a constant value (see Fig. 12). This is an interesting point since it shows that the dynamics and feedback control yield flight conditions close to the ones of real helicopters which fly with a constant $\dot{\gamma}$ thanks to a local regulation feedback of the main rotor speed (which does not exist on the VARIO scale model helicopter).

We apply the control in (28) for all $t \geqslant 0$. If the initial data are chosen as $z(0)=L, z^{(j)}(0)=0$ for all $j \geqslant 1$ (the helicopter is at rest on the ground); and if $z_d = L$, then the first error equation in (29) becomes $z - z_d = 0$. The dynamics when the constraint $z = L$ is activated is given for the z-coordinate by

$$0 = c_8\dot{\gamma}^2 u_1 + c_9\dot{\gamma} + c_{10} - c_7 - \lambda \tag{33}$$

with $\lambda \geqslant 0$ the reaction of the ground. Under the stated conditions (initial values and active unilateral constraint) it is easy to see that the control

$$u_1 = \frac{1}{c_8\dot{\gamma}^2}[c_7 - c_{10} - c_9\dot{\gamma} + v(t)] \tag{34}$$

implies $\lambda = v(t)$. One may choose the signal $v(t) \geqslant 0$ in a suitable fashion during the start-up period. When take-off is desired at $t = t_{\text{off}}$ one has to design $v(t) = 0$ and $z_d(t) < L$ for $t \geqslant t_{\text{off}}$.

To use this control strategy an initial minimal value of the main rotor angular speed ($\dot{\gamma}_0$) has to be guaranteed to avoid initial saturation on the control $u_{\text{m}}^1 \leqslant u_1 \leqslant 0$ and $u_{\text{m}}^2 \leqslant u_2 \leqslant u_{\text{M}}^2$. Here $u_{\text{m}}^1 = -0.0112$ m, $u_{\text{m}}^2 = -0.005$ m and $u_{\text{M}}^2 = 0.005$ m. From the second equation in (28) and assuming $\ddot{\phi} = \dddot{\phi} = \tilde{\phi} = 0$ we have:

$$\begin{aligned} u_{\text{M}}^2 > \frac{1}{c_5 c_{11}\dot{\gamma}_0^2}[&2c_5c_6\sin(2c_3\gamma_0)\dot{\gamma}_0\dot{\phi}_0 \\ &+c_4((c_{12}\dot{\gamma}_0 + c_{13})u_1 + c_6\sin(2c_3\gamma_0)\dot{\phi}_0^2 \\ &+c_{14}\dot{\gamma}_0^2 + c_{15})], \end{aligned} \tag{35}$$

where u_{M}^2 is the upper limit of the u_2 control saturation and the index 0 refers to initial conditions. Neglecting the terms containing $\dot{\phi}$ a sufficient condition to respect u_2 saturations in (28) is given by:

$$(c_{14} - c_5c_{11}u_{\text{M}}^2)\dot{\gamma}_0^2 + c_4c_{12}u_1\dot{\gamma}_0 + c_4c_{13}u_1 + c_{15} > 0. \tag{36}$$

From (28) and using the zero-dynamics stability analysis one can say that if $\dot{\gamma}(0)$ is large enough then the input is likely to be kept within the saturation limits. Simulation results confirm this intuitive reasoning.

Parametric robustness with respect a, c_{d} and K_{mot} will be numerically studied for this linearizing controller by computing the quadratic criterion in (22).

5. Simulation results

5.1. Take-off and vertical flight

In this section we present some numerical results obtained for the 3-DOF model for the I/O linearizing control strategy described previously. We impose the take-off time at $t_{\text{off}} = 50$ s and we use the following desired trajectory:

$$\begin{aligned} z_{\text{d}} &= -0.2, && 0 \leqslant t \leqslant t_{\text{off}}, \\ z_{\text{d}} &= 0.3[\text{e}^{-(t-t_{\text{off}})^2/350} - 1] - 0.2, && t_{\text{off}} < t \leqslant t_a, \\ z_{\text{d}} &= 0.1\cos[(t-130)/10] - 0.6, && t_a < t < t_b, \\ z_{\text{d}} &= -0.5, && t \geqslant t_b, \end{aligned}$$

where $t_a = 130$ s, $t_b = 20\pi + 130$ s and

$$\begin{aligned} \phi_{\text{d}} &= 0, && t < t_{\text{off}}, \\ \phi_{\text{d}} &= 1 - \text{e}^{-(t-t_{\text{off}})^2/350}, && t_{\text{off}} \leqslant t < t_c, \\ \phi_{\text{d}} &= \text{e}^{-(t-120)^2/350}, && t_c \leqslant t < t_d, \\ \phi_{\text{d}} &= -1 + \text{e}^{-(t-180)^2/350}, && t \geqslant t_d, \end{aligned}$$

where $t_c = 120$ s, $t_d = 180$ s. In this section we present two simulations. The first one is defined by the following initial conditions:

- $z(0) = -0.2$ m, $\dot{z}(0) = 0$ m/s.
- $\phi(0) = -\pi$ rad, $\dot{\phi}(0) = 0$ rad/s.
- $\gamma(0) = -\pi$ rad, from (36) and assuming that $\ddot{z}(0) = \dddot{z}(0) = \tilde{z}(0) = 0$ we have $\dot{\gamma}(0) = -99.5$ rad/s.

Initial conditions for the second simulation are:

- $z(0) = -0.2$ m, $\dot{z}(0) = 0$ m/s.
- $\phi(0) = \pi$ rad, $\dot{\phi}(0) = 0.2$ rad/s.
- $\gamma(0) = -\frac{3}{2}\pi$ rad, $\dot{\gamma}(0) = -50$ rad/s.

In Fig. 9 one can see the altitude and the yaw angle variation for both simulations.

As one can see in Fig. 10 and from initial conditions when $\|\dot{\gamma}(0)\|$ decreases, the u_2 control input saturates at the beginning of the simulation with a worse behavior. Nevertheless the stability of the closed-loop system is not destroyed. The u_1 control input behavior is practically the same for both simulations. Errors in the altitude and in the yaw angle are provided in Fig. 11.

One can see in Fig. 12 that the main rotor thrust converges to the value that compensates for the weight and for the drag force on the helicopter fuselage. In this figure one observe that $\dot{\gamma} \to -124.62$ rad/s as expected from the previous stability analysis.

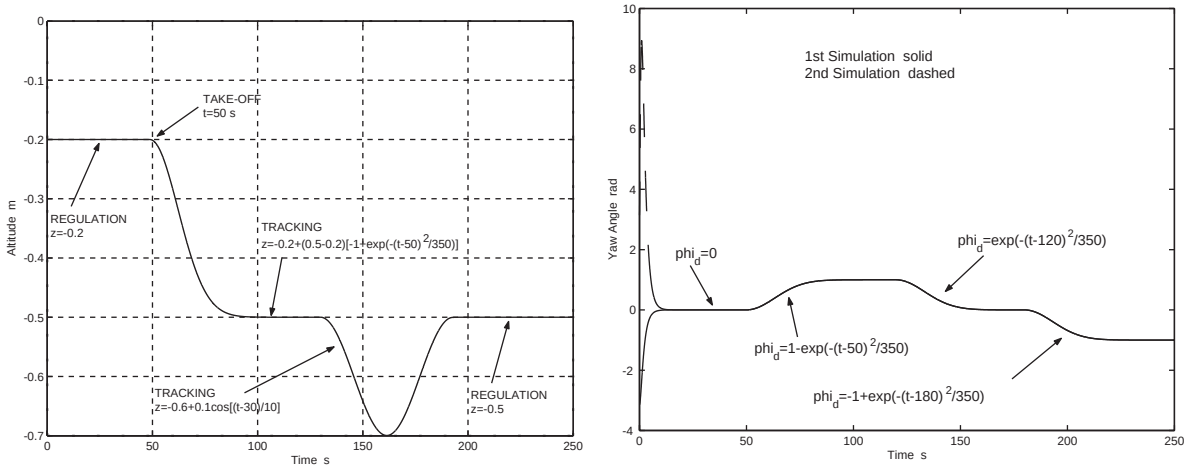

Fig. 9. z and ϕ behavior.

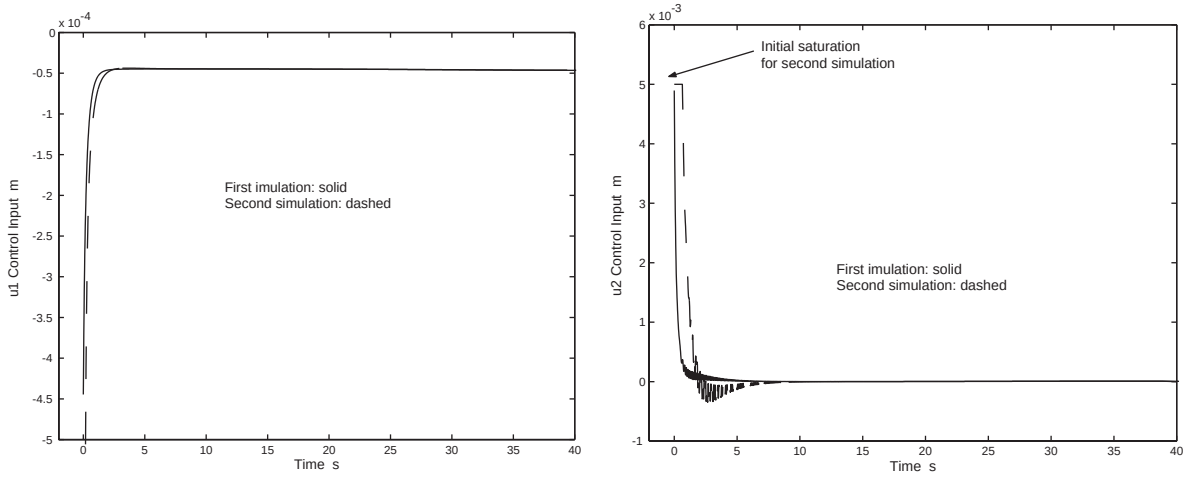

Fig. 10. u_1 and u_2 behavior.

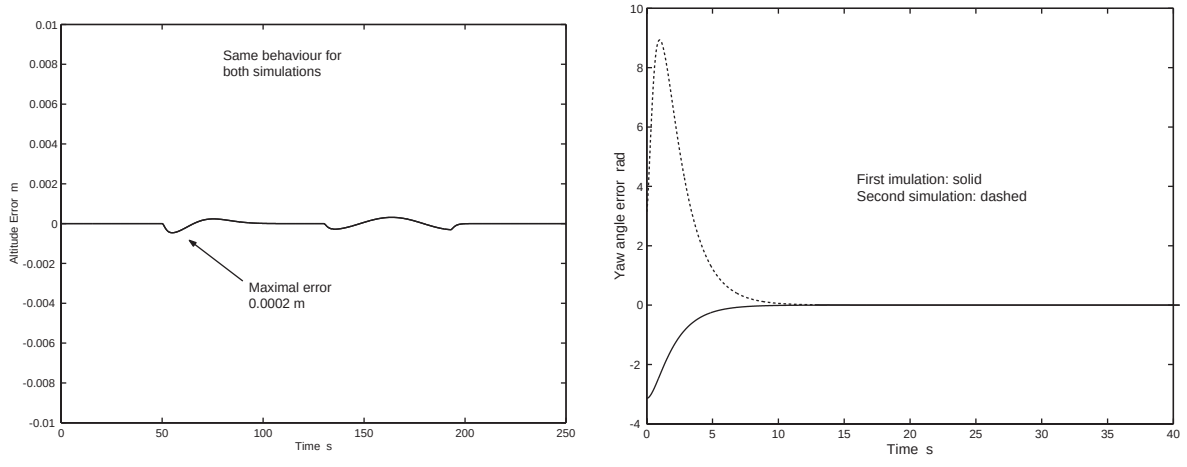

Fig. 11. $\tilde{z}$ and $\tilde{\phi}$ convergence to zero.

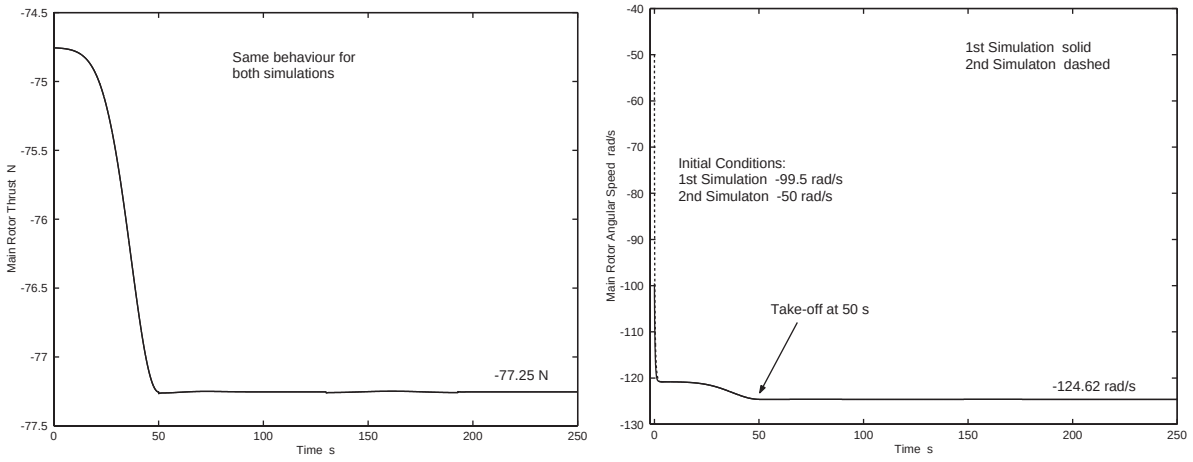

Fig. 12. T_M and $\dot{\gamma}$ behavior.

The main rotor angular speed behavior before the take-off time is due to the $v(t)$ signal used on (34) where:

$$v(t) = -2.5[-1 + e^{-(t-t_{off})^2/350}], \quad 0 \leqslant t < t_{off},$$
$$v(t) = 0, \quad t \geqslant t_{off}.$$

Remark 4. Some other simulation experiments have been performed with different desired trajectories ($\phi_d = 0$, for $t < t_{off}$ and $\phi_d = \frac{\pi}{4}[1 - \cos((t - t_{off})/10)]$, for $t \geqslant t_{off}$, for instance) and different initial conditions. In all cases the main rotor angular speed converges in a quite similar way to the same value ($\dot{\gamma} \to -124.62$ rad/s).

Remark 5. The numerical results show that the choice of the desired trajectories is a crucial step in helicopter control design. It is expected that this will be even more important for the control of the 7-DOF model when a disturbance (wind blow) suddenly drives the helicopter away from its desired position/orientation. Then a specific orbit will have to be designed in order to control the helicopter towards its original position/orientation, without saturating the inputs. At this stage the overall control problem will necessarily involve a module for the on-line design of such desired trajectories.

5.2. Parametric robustness

The estimated values of the parameters a, c_d and K_{mot} which are used in the model are $a = 5.73$, $c_d = 0.01$ and $K_{mot} = 100,000$ N. The parameters a and c_d depend on the airfoil of the main rotor blades. This values correspond to a NACA[5] 2412 airfoil (Abbott & Von Doenhoff, 1949) that is approximately the VARIO main rotor blades airfoil.

We have tested the robustness of the designed controller with respect to three parametric uncertainties on a, c_d and K_{mot} using the criterion defined in Eq. (22) while performing the first simulation previously defined. We perform simulations with the above nominal parameters with an uncertainty interval of $\pm 10\%$. In Table 2 one can see the percentage variation of J when the three parameters are varying of $\pm 10\%$. In this table J_j represents the variation of the criterion with respect to the parameter $j = a, c_d, K_{mot}$.

Table 2
Criterion variations

Variation	J_a	J_{c_d}	$J_{K_{mot}}$
$+10\%$	-1.121×10^{-5}	1.626×10^{-7}	-0.252
-10%	-10.47	-1.523×10^{-7}	-1.184×10^{-6}

When a is varying of -10%, when K_{mot} is varying of $+10\%$ and when the three parameters are varying simultaneously of -10% the input u_2 saturates at the beginning of the simulation. The input u_1 and the others variables have acceptable behavior. For the rest of the parametric variations all the variables behaviors are acceptable. We can say from these numerical results that this controller has some robustness properties with respect to the c_d and K_{mot} uncertainties.

We can see that an overestimation of a is preferable to an underestimation in order to assure partial parametric robustness of this controller with respect to the a parameter.

6. Real-time experiments in a vertical flying stand

Fig. 13 shows the platform used in experiments with the Vario helicopter. We have experimentally observed that the helicopter takes off at 1550 r.p.m. and that the rotor angular speed remains practically constant for the vertical displacement allowed in the platform. From model (13), (15) and (17) the equation for z can be rewritten as follows (see also (25) for $\lambda = 0$):

$$m\ddot{z} = c_8\dot{\gamma}^2 u_1 - mg, \tag{37}$$

[5] NACA is the National Advisory Committee for Aeronautics.

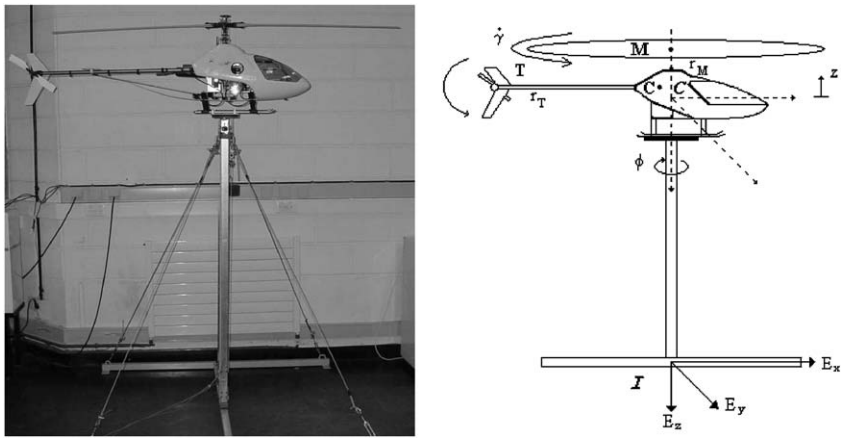

Fig. 13. Helicopter-vertical platform.

where $mg \simeq c_9\dot{\gamma} + c_{10} - c_7$, m is the helicopter mass (i.e. 7.5 kg), $\dot{\gamma} \approx 1550$ r.p.m. is the rotor angular speed, u_1 is the blades collective pitch angle and g is the gravitational acceleration. We have experimentally observed that c_8 is such that $mg/c_8\dot{\gamma}^2$ lies in the interval [1.6,2.0].

From the second and third rows of model (13), (15) and (17) neglecting c_2 and c_6 since they are very small, and solving for $\ddot{\phi}$ we get:

$$(c_1c_5 - c_4^2)\ddot{\phi} = c_5c_{11}\dot{\gamma}^2(u_2 - k_g\dot{\phi}) - c_4[(c_{11}\dot{\gamma} + c_{13})u_1 + c_{14}\dot{\gamma}^2 + c_{15}], \quad (38)$$

where the term $-k_g\dot{\phi}$ comes from an angular velocity feedback of the gyro control system for the tail of the helicopter. This angular velocity feedback is part of the helicopter and has not been removed.

We have calculated some of the coefficients in the above equation and we have experimentally obtained the rest of them. The estimated model is as follows:

$$k_1\ddot{\phi} = k_2u_2 - k_3\dot{\phi} - k_4, \quad (39)$$

where $k_1 = 0.43$, $k_2 = 206$, $k_3 = 4.3$ and $k_4 = 546$.

6.1. Controller design

The control strategy that we proposed in this paper is to use the control input u_1 to control the altitude z in such a way that (37) becomes (see (29)):

$$m\ddot{z} = -a_1\dot{z} - a_2(z - z^{\mathrm{d}}) \quad (40)$$

where $a_1 = m\lambda_1$ and $a_2 = m\lambda_2$ are positive constants and z^{d} is the desired altitude. From (37) and (40) u_1 is given by

$$u_1 = \frac{1}{\bar{c}_8\dot{\gamma}^2}[mg - a_1\dot{z} - a_2(z - z^{\mathrm{d}})]. \quad (41)$$

The control u_2 is computed in (38) such that the closed-loop system is (see also (29)):

$$k_1\ddot{\phi} = -a_3\dot{\phi} - a_4(\phi - \phi^{\mathrm{d}}), \quad (42)$$

where $a_3 = k_1\lambda_3$ and $a_4 = k_1\lambda_4$ are positive constants and ϕ^{d} is the desired yaw angle. Therefore u_2 is given by

$$u_2 = \frac{1}{k_2}[k_3\dot{\phi} + k_4 - a_3\dot{\phi} - a_4(\phi - \phi^{\mathrm{d}})]. \quad (43)$$

The control parameters a_1 and a_2 in (40) should be carefully chosen to avoid impacts between the helicopter and the platform when $z = 0$.

6.2. Experimental results

6.2.1. Hardware

The radio-controlled helicopter is a VARIO 1.8 diameter rotor with a 23 cm^3 gasoline internal combustion engine. The radio is a Graupner MC-20. The vertical displacement is measured by a linear optical encoder and the yaw angle is obtained through a standard angular encoder. The radio and the PC (INTEL Pentium 3) are connected using data acquisition cards (ADVANTECH PCL-818HG and PCL-726). In order to simplify the experiments the control inputs can be independently commuted between the automatic or the manual control modes. The connection in the radio is directly made to the joystick potentiometers for the gas and yaw controls. The vertical displacement of the helicopter in the platform varies from 1.8 to 2.5 m. Otherwise it can turn freely around the vertical axis. The angular velocity feedback $-k_g\dot{\phi}$ is carried out by the internal gyro control system of the helicopter.

6.2.2. Experiment

The vertical speed $\dot{z}$ is numerically estimated from the z measurement by simply setting

$$\dot{z}_t = \frac{z_t - z_{t-T}}{T}. \quad (44)$$

The gain values used for the control law are $a_1 = 0.01$, $a_2 = 0.08$, $a_3 = 0.1$ and $a_4 = 0.1$. The experiment considers the case of the stabilization of the helicopter-platform dynamics for various values of the altitude and yaw. The desired value

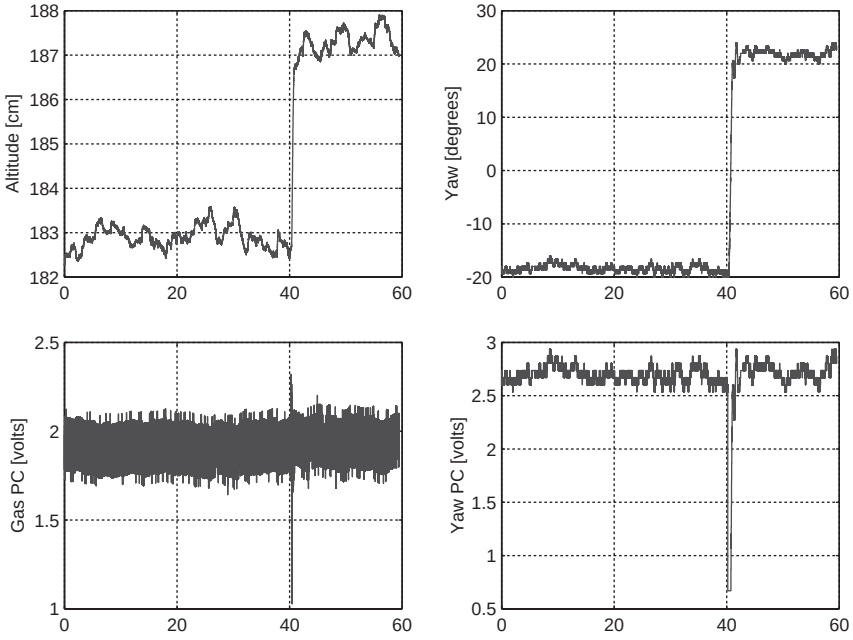

Fig. 14. Behavior of the altitude, yaw, inputs u_1 and u_2.

for the altitude is 4 cm from $t = 0$ to 40 s and 8 cm for $t \geqslant 40$ s. The desired yaw angle is $-20°$ from $t = 0$ to 40 s and $20°$ for $t \geqslant 40$ s.

Fig. 14 shows the performance of the controller when applied to the real helicopter in the vertical platform. In this figure the terms *Gas PC* and *Yaw PC* on vertical axes refer to the altitude/gas control u_1 and to the yaw control u_2, respectively and computed by the personal computer.

7. Conclusions

In this paper we have considered the modelling and the feedback control of a scale model helicopter. When the helicopter is mounted on a platform, the resulting model is an underactuated 3-DOF Lagrangian system, with 2 inputs. Some aerodynamical effects have been incorporated in the model to obtain the generalized torques as a function of the inputs (the swashplate displacements of the main and tail rotors) and of the main rotor angular velocity. The complete model also incorporates the transition from the constrained mode (the helicopter is at rest on the ground) to the flying mode (the helicopter is airborne). The way the generalized forces depend on the input is shown to be nonlinear, so that the resulting control problem is likely to be different from what is usually considered in the literature on mechanical systems control. A control strategy for the 3-DOF model based on a linearizing controller is used with an acceptable closed-loop system behavior and the stability of the zero-dynamics has been analyzed. Mechanical and aerodynamical coupling effects are taken into account in the model and in the control action. Numerical simulations and experimental applications on the VARIO scale model helicopter are presented to show the performance and robustness of the proposed controller. Further work will concern the control of the 7-DOF helicopter whose model can be found in Avila-Vilchis et al. (2000).

Acknowledgements

We would like to thank A. Desopper (ONERA Salon de Provence, France) for faithful discussions on the nonlinear and aerodynamical modelling. This work was performed while the first two authors were at the Laboratoire d'Automatique de Grenoble, France.

Appendix A. Aerodynamics

With the interest to clarify the presentation we provide the following glossary where some notions are explained. We use the figures in Section 2 to help the reader to understand some other aerodynamical terms. For more details the reader can consult Avila-Vilchis (2001), Prouty (1995) or Stepniewsky (1984).

$$\beta(\gamma) = a_0 - a_{1s}\cos\gamma - b_{1s}\sin\gamma. \tag{A.1}$$

where we have used the following notation of the main text:

a: The lift-curve slope per degree of the wing. It can be seen as $\mathrm{d}c_l/\mathrm{d}\alpha$ with c_l the section lift (aerodynamical) coefficient and α the section angle of attack (see Fig. 3). The lift coefficient depends on the main rotor blade airfoil.

a_0: The coning angle (see Fig. 7). It is related to the flapping equation of motion by Eq. (A.1) where a_{1s} and b_{1s} are the longitudinal and lateral flapping angles, respectively, and γ is the azimuth angle of the main rotor blades. In hover mode, the flapping angle is equal to the coning angle representing the form that the rotor blades take under the effect of the blades flexibility when they are rotating.

c: The chord of the main rotor blades. For a rectangular airfoil it represents the width of the blade (Fig. 3).

D_{vi}: The drag force produced by the main rotor wake. This force acts on the helicopter fuselage.

ΔD: The drag force increment produced by the relative speed of the air over the blade. This force depends on the drag (aerodynamical) coefficient c_{d} of the blade airfoil.

ΔL: The main rotor lift force increment depending on the blade airfoil and on the dynamical pressure (see Eq. (1)).

V_{T}: The tangent (relative) velocity to the blade element chord (see Fig. 4).

V_{P}: The perpendicular (relative) velocity to the blade element chord (see Fig. 4).

v_i: The induced velocity produced by the main rotor wake with $i = local$ for the blade element, $i = v$ for the vertical flight mode and $i = h$ for the hover mode.

u_1: The collective pitch angle (swashplate displacement) of the main rotor (see Fig. 7). This is the first control input.

u_2: The collective pitch angle (swashplate displacement) of the tail rotor (see Fig. 7). This is the second control input.

u_3: The longitudinal pitch angle of the main rotor. This is the third control input (case of the 7-DOF system).

u_4: The lateral pitch angle of the main rotor. This is the fourth control input (case of the 7-DOF system).

α: The main rotor blades angle of attack (see Fig. 3).

α_s: The main rotor angle of attack (see Fig. 4).

β: The flapping angle. Flapping phenomenon is a harmonic one constituted of a coning angle and a first harmonic motion (see Eq. (A.1)).

δ: The lateral angle of the helicopter translation (see Fig. 4).

$\imath_e$: The incidence angle (see Fig. 5).

φ: The blade pitch angle (see Fig. 3).

φ_1: In the blade pitch angle Eq. (4), the blade linear twist angle φ_1 represents the twist of the blade with respect to the radial distance r_e. R_{M} is the main rotor radius.

References

Abbott, I. H., & Von Doenhoff, A. E. (1949). *Theory of wing sections*. New York: Dover.

Avila-Vilchis, J. C. (2001). *Modélisation et commande d'hélicoptère*. Ph.D. thesis. INPG, France.

Avila-Vilchis, J. C., & Brogliato, B. (2000). Nonlinear passivity-based control for a scale model helicopter. In *26th European Rotorcraft Forum*. The Hague, The Netherlands.

Avila-Vilchis, J. C., Brogliato, B., & Lozano, R. (2000). *Modélisation d'hélicoptère*. Technical Report AP 00-021, Laboratoire d'Automatique de Grenoble, INPG, France.

Kaloust, J., Ham, C., & Qu, Z. (1997). Nonlinear autopilot control design for a 2-dof helicopter model. *IEE Proceedings on Control Theory and Applications*, *144*(6), 612–616.

Khalil, H. K. (1996). *Nonlinear systems* (2nd ed.). Englewood Cliffs, NJ: Prentice-Hall.

Kienitz, K., Wu, Q., & Mansour, M. (1990). Robust stabilization of a helicopter model. In *Proceedings of the 29th Conference on Decision and Control*, Honolulu, Hawaii, USA, (pp. 2607–2612).

Koo, T. J., Hoffmann, H., Sinopoli, B., & Sastry, S. (1998). Hybrid control of an autonomous helicopter. In *Preprints of the third IFAC International Workshop on Motion Control*, Grenoble, France, (pp. 285–290).

Koo, T. J., & Sastry, S. (1998). Output tracking control design of a helicopter model based on approximate linearization. In *37th IEEE Conference on Decision and Control*, Tampa, FL, USA.

Mahony, R., & Lozano, R. (1999). An energy based approach to the regulation of a model helicopter near to hover. In *European Control Conference*, Karlsruhe, Germany.

McCormick, B. W. (1995). *Aerodynamics, Aeronautics and Flight Mechanics*. New York: Wiley.

Mukherjee, R., & Chen, D. (1993). Control of free-flying underactuated space manipulators to equilibrium manifolds. *IEEE Transactions on Robotics and Automation*, *9*(5), 561–570.

Phillips, C., Karr, C. L., & Walker, G. (1996). Helicopter flight control with fuzzy logic and genetic algorithms. *Engineering Applications in Artificial Intelligence*, *2*(9), 175–184.

Prouty, R. W. (1995). *Helicopter performance, stability and control*. New York: Krieger.

Reyhanoglu, M., Van der Schaft, A., McClamroch, N. H., & Kolmanovsky, I. (1999). Dynamics and control of a class of underactuated mechanical systems. *IEEE Transactions on Automatic Control*, *44*(9), 1663–1671.

Rozak, J. N., & Ray, A. (1997). Robust multivariable control of rotorcraft in forward flight. *American Helicopter Society*, *43*(3), 149–160.

Shim, H., Koo, T. J., Hoffman, F., & Sastry, S. (1998). A comprehensive study of control design for an autonomous helicopter. In *37th IEEE Conference on Decision and Control*, Tampa, FL, USA.

Sira-Ramírez, H., Zribi, M., & Ahmed, S. (1994). Dynamical sliding mode control approach for vertical flight regulation in helicopters. *IEE Proceedings on Control Theory and Applications*, *141*(1), 19–24.

Stepniewsky, W. Z. (1984). *Rotor-wing aerodynamics, Basic Theories of Rotor Aerodynamics*. New York: Dover.

Tchen-Fo, F., Allain, C., & Desopper, A. (2000). Improved vortex ring model for helicopter pitch up prediction. In *26th European Rotorcraft Forum*, The Hague, The Netherlands.

Juan Carlos Avila Vilchis was born in Toluca, Mexico. He received in 1988 his B.S. degree in Mechanical Engineering from the Autonomous University of the State of Mexico (UAEM). He got in 1990 a master degree in Mechanical Engineering from the Central School of Lille (ECL), France. He received his M.S. and Ph.D. degrees in Automatic Control from the Polytechnical National Institute of Grenoble (INPG), France, in 1998 and 2001, respectively. From 2001 to 2002, he was a research fellow of the Automatic Control Laboratory of Grenoble (LAG), France. From January to August 2003 he was an associate research engineer of the TIMC laboratory at the Joseph Fourier University (UJF), France. He is an Associate Professor at the Faculty of Engineering of the UAEM. Nonlinear dynamics and control and medical robotics are his current research interests.

Bernard Brogliato is working at the INRIA Rhône-Alpes in Grenoble (the French National Institute for Research in Computer Science and Control). His main activities concern non-smooth dynamical systems analysis, modeling, and control. He is Associate Editor for Automatica, reviewer for Mathematical Reviews and ASME Applied Mechanics Reviews. He is a member of the Euromech Nonlinear Oscillations Conference Committee (ENOCC), and of the European Union of Control Associations (EUCA) council.

Alejandro Dzul was born in Gmez Palacio, Mexico, on April 30, 1971. He received his B.S degree in Electronic Engineering in 1993 and his M.S. degree in Electrical Engineering in 1997 from La Laguna Institute of Technology, and the Ph.D. degree in Automatic Control from Université de Technologie de Compiègne, France on November 2002. He is Research Professor in the Electrical and Electronic Engineering Department, at La Laguna Institute of Technology since January 2003. His currently research interests are in the areas of nonlinear dynamics and control, and real time control with applications to aerospace vehicles.

Rogelio Lozano was born in Monterrey Mexico, on July 12, 1954. He received the B.S. degree in electronic engineering from the National Polytechnic Institute of Mexico in 1975, the M.S. degree in electrical engineering from Centro de Investigacion y de Estudios Avanzados (CIEA), Mexico in 1977, and the Ph.D. degree in automatic control from Laboratoire d'Automatique de Grenoble, France, in 1981. He joined the Department of Electrical Engineering at the CIEA, Mexico, in 1981 where he worked until 1989. He was Head of the Section of Automatic Control from June 1985 to August 1987. He has held visiting positions at the University of Newcastle, Australia, from November 1983 to November 1984, NASA Langley Research Center VA, from August 1987 to August 1988, and Laboratoire d'Automatique de Grenoble, France, from February 1989 to July 1990. Since 1990 he is a CNRS Research Director at University of Technology of Compiègne, France. He is head of the Laboratory Heudiasyc, UMR 6599 CNRS since January 1995. Dr Lozano was Associate Editor of Automatica from 1987 to 2000 and of Int. J. of Adaptive Control and Signal Processing since 1993. His research interest are in adaptive control, passivity, nonlinear systems, underactuated mechanical systems and autonomous helicopters.